Superior toughened bio-compostable Poly(glycolic acid)-based blends with enhanced melt strength via selective interfacial localization of in-situ grafted copolymers

Deyu Niu [a], Pengwu Xu [a], Zhaoyang Sun [b], Weijun Yang [a], Weifu Dong [a], Yang Ji [b], Tianxi Liu [a], Mingliang Du [a], Pieter Jan Lemstra [a,c], Piming Ma [a,*]

[a] The Key Laboratory of Synthetic and Biological Colloids, Ministry of Education, Jiangnan University, 1800 Lihu Road, Wuxi, 214122, China
[b] Inner Mongolia Pujing Polymer Material Technology Corporation Ltd, Baotou, Inner Mongolia, 014060, China
[c] PlemPolco B.V, De Zicht 11, 5502, HV Veldhoven, the Netherlands

A B S T R A C T

As an emerging bioplastic, poly(glycolic acid) (PGA) possesses excellent bio-compostability, gas barrier properties, mechanical strength and heat resistance. However, the inherent brittleness and inferior melt-strength of PGA severely limits its processability and application possibilities. In the present contribution, a two-step reactive melt blending of PGA and poly(butylene adipate-co-terephthalate) (PBAT) with epoxy functionalized copolymer (ethylene-methyl acrylate-glycidyl methacrylate) (EMAG) as compatibilizer was investigated to solve these shortcomings. The EMAG was first blended with PBAT and then with PGA to in-situ form PGA-g-EMAG-g-PBAT copolymers. These copolymers selectively locate at the interface between PGA and PBAT, which effectively improved the interfacial adhesion and the compatibility. Consequently, the PGA/(PBAT/EMAG) blends with 1 wt % EMAG exhibited high elongation at break ($45 \pm 4\%$) and a notched impact strength (14.4 ± 1.6 kJ/m^2) respectively, which is about 1100% and 410% higher than that of PGA. Meanwhile, the viscosity and storage modulus of the PGA/(PBAT/EMAG) blends at 50.1 Hz were enhanced by 130% and 230% compared with PGA. This work provides a facile route to fabricate PGA-based blends with excellent toughness and melt strength, which could open up new possibilities for the application of PGA materials.

1. Introduction

Over the past few decades, the production and application of bioplastic has been developing and evolving rapidly due to growing environmental awareness [1] [–] [4]. Poly(glycolic acid) (PGA) is a bio-compostable aliphatic polyester exhibiting good biocompatibility and high performance regarding e.g., the superior barrier properties [5]. PGA can be obtained either from biomass, such as microbial fermentation of pineapple or sugarcane, or chemically synthetic routes using methanol as the starting material [6] [–] [8]. However, the traditional routes of PGA synthesis often involve corrosive and toxic Cl or HCN impurities makes it not suitable for environmental-friendly production in large scale [6]. Thus PGA was quite expensive for a long time and it was mainly used in high value-added products in the biomedical field, e. g., surgical sutures [9], drug delivery carriers [10], wound closure and bone fixation materials [11]. In recent years, a new polymerization

route of PGA was developed and the low-cost PGA was successfully industrialized by Pujing Co., China. This development will promote the PGA into a wider range of industrial applications such as food packaging.

PGA possesses excellent barrier properties for permanent gases, mechanical strength and heat resistance, which makes PGA outstanding and competitive to petroleum-based polymers like PET, EVOH, or Nylon in high-barrier packaging applications [5,12]. Unfortunately, the elongation at break and the notch impact strength of PGA are less than 10% and 4 kJ/m^2, respectively. This inherent brittleness is the major obstacle for a wider application of PGA. Several strategies including copolymerization, plasticization, and blending have been used in general to conquer the brittleness of polymer materials. Blending with flexible polymers such as natural rubbers, elastomers, acrylic impact modifiers, polyethylene (PE) is considered the most convenient and economical method [13] [–] [20]. But most of these flexible polymers are

* Corresponding author.
E-mail address: p.ma@jiangnan.edu.cn (P. Ma).

non-compostable. Poly(butylene adipate-co-butylene terephthalate) (PBAT) is classified as a compostable polyester with excellent flexibility and could be the preferred candidate for toughening PGA without compromising on the biocompostability [21,22]. However, recent investigations have shown that PGA/PBAT blends exhibit unsatisfactory mechanical properties due to lack of sufficient compatibility and, consequently, weak interface interaction [23].

The compatibility can be enhanced by increasing interface interaction between components via physical and chemical methods such as the use of so-called compatibilizers. For example, polylactic acid - polyethylene glycol - polylactic acid (PLA-PEG-PLA) tri-block copolymer was used as a compatibilizer for PLA/PBAT blends. The different blocks of the copolymers are miscible with PLA and PBAT phase, respectively. So the interfacial interactions between PLA and PBAT was enhanced by the tri-block copolymer through physical interaction [24]. But the design and synthesis process of block copolymers are quite complex and expensive. Meanwhile, the compatibilization efficiency is not so high based on physical interaction. Reactive blending is a simple and effective compatibilization technology, providing in-situ formed chemical bonding between components to improve the interfacial interaction [25]. The chemical bonds are much stronger than physical interactions and the compatibilization efficiency is higher. Several studies have demonstrated that adding reactive compatibilizers can improve the compatibility between two components, thus enhancing the mechanical performance of blends [26–28]. The literature survey suggest that the reactive compatibilizers of polyester systems mainly included the free-radical initiator such as dicumyl peroxide (DCP) [29,30], the compounds or polymers with multiple anhydride groups [31], isocyanate groups [32] or epoxy groups [33–35]. Among them, the free-radical initiator may cause degradation of polyesters. The undesirable toxicity and volatility of the isocyanate compounds and the poor reactivity of anhydride groups limit the application. The most widely used reactive compatibilizers are compounds or polymers containing multi-epoxy groups. ADR (a multifunctional epoxy oligomers) was used as compatibilizer to prepare tough PLA/PBAT blends. The notched impact strength and the elongation at break of blends were reported to be 75 and 12 times higher than PLA, which were attributed to the in-situ formed PLA-PBAT copolymers [36]. Chang et al. [37] demonstrated that the mechanical properties of the PLA/PBT blends were improved by utilizing an epoxidized styrene-acrylic (ESAC) and ethylene-n-butyl-acrylate-co-glycidyl methacrylate (EBA-GMA). The ESAC and EBA-GMA have a synergistic compatibilizing effect, which contributes to the notched impact strength enhancement by more than 200%. As far as we are aware of, there are only a few investigations regarding the compatibilization effect of polymers with multi-epoxy groups on PGA-based blends. Furthermore, it's worth noting that the degree of dispersion and location of compatibilizer has a significant influence on the efficiency of compatibilization and thus mechanical properties for multicomponent blends [38,39]. Obviously, when the compatibilizer is located at the interface between components, the compatibility is most effective. Wei et al. [40] used poly (styrene-co-glycidyl methacrylate) (SG) as the reactive compatibilizer to improve the interfacial adhesion between PLLA and PBAT. It was revealed that the SG-g-PBAT was completely located at the interface and presented the highest compatibilization effect. Consequently, the types and distribution of compatibilizers are critical issues to improve the compatibility and physical properties of PGA-based blends.

In the present work, we focus on toughening PGA with the commercially available flexible biodegradable polyester PBAT and an epoxy functionalized copolymer (ethylene-methyl acrylate-glycidyl methacrylate) (EMAG) was used as reactive compatibilizer. The PGA and PBAT are well-known bio-compostable according to the EN13432, and a small amount of EMAG is not expected to compromise this feature. In addition, the epoxy groups of EMAG can react with the terminal hydroxyl/carboxyl groups of both PGA and PBAT to improve interfacial interactions. By evaluating the interfacial interactions and reactivity
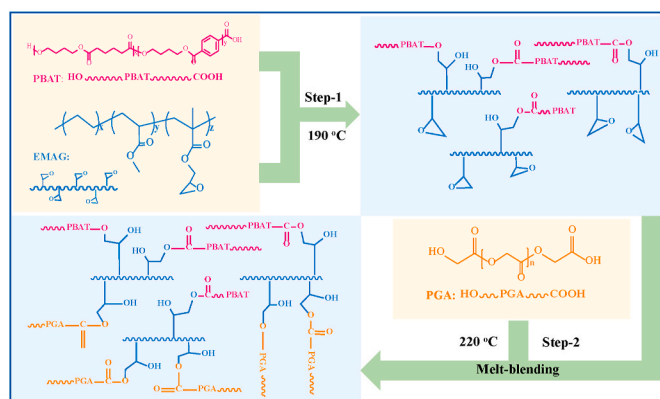
Scheme 1. Schematic diagram illustrating possible reaction mechanism between the polyester (PGA and PBAT) and EMAG via two-step blending process.

between the components, it is expected that EMAG tends to be dispersed in the PGA matrix. In order to control distribution of EMAG, a facile two-step blending method was designed to change reaction kinetics of PGA and PBAT grafted EMAG chain, so that the EMAG is selectively located at the interface to form stronger interfacial adhesion. The graft reaction, rheological performance, phase morphological and physical properties of PGA/(PBAT/EMAG) blends were systematically investigated. This work provides a new design and a facile route to process superior toughened PGA-based blends with high compatibilization efficiency. This novel route is expected to broaden the application range of PGA materials in packaging and other fields.

2. Experimental section

2.1. Materials

PGA ($M_w = 1.5 \times 10^5$ g/mol, $M_w/M_n = 1.5$) was supplied by Shanghai Pujing Chemical Industry Co. Ltd., China. PBAT ($M_w = 8.4 \times 10^4$ g/mol, $M_w/M_n = 1.3$) was obtained from Kingfa Sci. & Tech. Co. Ltd., China. The random copolymer of ethylene-methyl acrylate-glycidyl methacrylate (EMAG, E/MA/GMA = 68/24/8 (wt %), $M_w = 4.5 \times 10^4$ g/mol [39]) utilized as the reactive compatibilizer for the PGA/PBAT blend was purchased from Arkema Innovative Chemistry Co. Ltd., France.
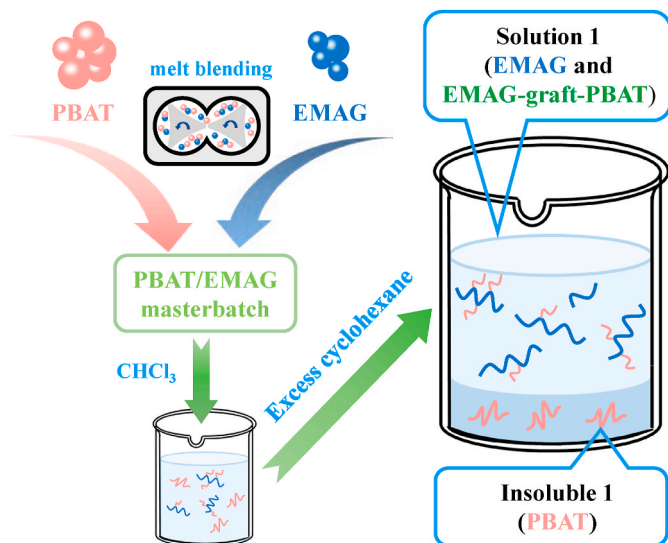
2.2. Sample preparation

The PGA, PBAT were dried at 70 °C under vacuum overnight and the EMAG was dried for 24 h at 45 °C before blending.

Route 1: Blends of PGA/PBAT/EMAG (named as a one-step processing) were performed using a Haake rheometer (Polylab-OS) operating at 220 °C and 60 rpm for 6 min. For comparison, PGA, PGA/PBAT samples were prepared using the same procedure.

Route 2: First, PBAT/EMAG mixtures were made by using the Haake rheometer at 190 °C and 60 rpm for 6 min. Subsequently, the PBAT/EMAG mixtures were compounded with only PGA by using the Haake rheometer at 220 °C and 60 rpm for 6 min to prepare PGA/(PBAT/EMAG) ternary blends (named as a two-step processing). The anticipated reaction mechanism involved in the two-step blending process is schematically illustrated in Scheme 1. To investigate the grafting reaction between PBAT and EMAG, PBAT/EMAG mixtures were prepared also at 210 °C and 230 °C, respectively.

The weight ratio of PGA/PBAT was designed as 70/30 in all ternary blends, while the weight percentage of EMAG was in the rage of 0–3% based on the total amount of PGA and PBAT. The samples were compression-moulded (at 220 °C and 10 MPa for 3 min) into sheets and quenched to room temperature subsequently for tensile, Izod impact,

Scheme 2. Schematic of the procedure for sample preparation for ^{1}H NMR characterization.

Table 1
Contact angle and surface tension date of the components.

Sample	Contact angle (deg)			Surface tension (mN/m)	
	water	diiodomethane	Total (γ)	Dispersion component (γ^d)	Polar component (γ^p)
PGA	88.8 ± 1.3	50.9 ± 2.4	34.22	32.03	2.19
PBAT	83.5 ± 1.6	37.7 ± 2.5	41.38	39.21	2.17
EMAG	78.3 ± 2.1	44.3 ± 2.7	37.44	31.36	6.08

Table 2
Interfacial tension, work of adhesion and spreading coefficient of polymer pairs.

polymer pairs	interfacial tension, α_{ij} (mN/m)	work of adhesion, W_{ij} (mN/m)	spreading coefficient, λ_{ij}
PGA/PBAT	0.36	75.24	$\lambda_{AC} = 0.03 > 0$
PGA/ EMAG	0.98	70.68	$\lambda_{BC} = -0.75 < 0$
PBAT/ EMAG	1.37	69.98	$\lambda_{CB} = -1.99 < 0$

rheology and DMA tests. For convenience, the PGA/(PBAT/EMAG) blends made by the two-step processing are coded as G/(B/EG*x*), while the PGA/PBAT blends and the PGA/PBAT/EMAG blends obtained by the one-step processing are represented as G/B and G/B/EG*x*, respectively, where the *x* represents the EMAG percentage of EMAG based on the total amount of PGA and PBAT in the ternary blends. For example, G/(B/EG3) meaning that in the weight ratio of PGA, PBAT and EMAG is 70/30/3 in the final PGA/(PBAT/EMAG) ternary blend.

2.3. Characterization

The interfacial interactions of the various samples were derived from the contact angle (water and diiodomethane). The reaction between PBAT and EMAG in the first-step was characterized by ^{1}H NMR (Bruker Advance 2B). The separation procedure of the sample used for the ^{1}H NMR characterization is shown in Scheme 2 and further details can be found in the Supporting Information. The morphology of the blends was studied using SEM (S-4800, HITACHI, Japan), TEM (200 kV, JEOLJEM-2100, Japan) and AFM (Multimode 8, Bruker Nano, USA). The rheological behavior of the blends was analyzed by DHR-2 rheometer (TA Instruments). The glass transition temperature of blends was investigated by DMA analyzer (Q800, TA, USA). The Instron 5967 testing instrument was utilized to determine mechanical response of blends. The thermal behavior of the blends was studied by DSC (PerkinElmer, USA). The details of each characterization are described in the Supporting Information.

3. Results and discussion

3.1. Determination the interactions and reactivity between the components

The interfacial interactions of samples were estimated by interfacial tension values, and the interfacial tension values were derived from the surface tension values which were calculated by using the contact angle (water and diiodomethane) method. The surface energy (γ) and its polar (p^p) and dispersion (γ^d) components of the samples were calculated according to Owens-Wendt method using the following equations [41]:

$$\gamma = \gamma^p + \gamma^d \tag{1}$$

$$(1+\cos\theta)\gamma_l = 2\sqrt{\gamma_s^p\gamma_l^p} + 2\sqrt{\gamma_s^d\gamma_l^d} \tag{2}$$

where the θ is the contact angle of the polymer with liquid, the subscripts "s" and "l" represent solids and liquids, respectively. It is widely reported that water and diiodomethane are used as test liquids [42]. The polar and dispersion components values are $\gamma^p_{H_2O} = 50.7$ mN/m, $\gamma^d_{H_2O} = 22.1$ mN/m, $\gamma^p_{CH_2I_2} = 6.7$ mN/m and $\gamma^d_{CH_2I_2} = 44.1$ mN/m, respectively. The contact angles of PGA, PBAT, EMAG with the water and diiodomethane and the values of surface tension calculated from the equations are listed in Table 1.

The following equations were used to calculate the interfacial tension (γ_{ab}) and the thermodynamic work of adhesion (W_{ab}) between polymers [41]:

$$\gamma_{ab} = \gamma_a + \gamma_b - 2\sqrt{\gamma_a^p\gamma_a^p} - 2\sqrt{\gamma_a^d\gamma_b^d} \tag{3}$$

$$W_{ab} = 2\sqrt{\gamma_a^p\gamma_a^p} + 2\sqrt{\gamma_a^d\gamma_b^d} \tag{4}$$

Furthermore, the thermodynamically stable morphology of the blends was predicted according to the spreading coefficient models. According to Hobbs et al. [43] in a ternary immiscible blend with constituents A, B and C, the spreading coefficient (λ_{CB}) can be defined as

$$\lambda_{CB} = \gamma_{BA} - \gamma_{CA} - \gamma_{BC} \tag{5}$$

where λ_{ij} is the spreading coefficient of i over j and it gives the tendency of i to spread at the interface of j. The γ_{ij} is the interfacial tensions between the different polymers. λ_{CB} must be positive for B to be encapsulated by C. One positive and two negative spreading coefficients indicate that the tendency of one phase to segregate the two other phases [44]. The three negative spreading coefficients is described as partial wetting. In this work, A is the PGA matrix, B is the PBAT and C is the EMAG. Interfacial tension, adhesion work and spreading coefficient are listed in Table 2. The interfacial tension between PBAT and EMAG is bigger than that of PGA/EMAG couple, indicating that PGA has a higher affinity to EMAG chains. The work of adhesion data further confirms this statement, as the PBAT/EMAG has the lowest work of adhesion. Table 2 shows that the λ_{AC} is positive, λ_{BC} and λ_{CB} are negative. It suggests that EMAG and PBAT will separate and EMAG will be encapsulated by the PGA matrix in a PGA/PBAT/EMAG ternary blend.

It should be emphasized that the formation of block or graft copolymers by in-situ reaction will greatly reduce the interfacial tension by more than 70% [45]. In this work, the in-situ reaction between EMAG,
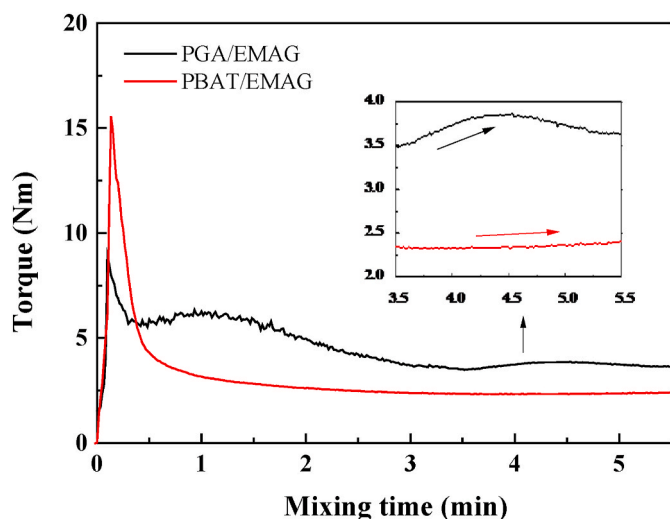
Fig. 1. Melt torque evolution over mixing time for PGA/EMAG (70/30) and PBAT/EMAG (70/30) blends processed at 220 °C.

PGA and PBAT will reduce the interfacial tension and thus changing the phase morphology. However, the in-situ formed copolymers might mainly become encapsulated within one phase if there is a large difference in the reaction rates between the PGA and the PBAT with EMAG chains, leading to inefficient compatibilization effect. The differences in reactivities of EMAG with PGA and PBAT can be investigated by the evolution of torque [46–48]. The torque evolution over mixing time for

PGA/EMAG (70/30) and PBAT/EMAG (70/30) is shown in Fig. 1. The torque curve of PGA/EMAG shows two peaks before 3 min. The first peak is attributed to the feeding process and the melting of the EMAG. The peak at about 1 min is corresponding to the melting and plasticizing processess of PGA, because the plasticizing process of PGA is slow in this work due to a relatively low processing temperature (220 °C), see also the torque peak of neat PGA in Fig. S1. More importantly, the torque of PGA/EMAG blend increases after 3 min as the time increased because of the in situ formed copolymers. For comparison, the torque of PBAT/E-MAG blend do not increase. It is shows that the reaction in PGA/EMAG is faster than in PBAT/EMAG. The EMAG component prefers to react with PGA in the melt blending of PGA, PBAT and EMAG. The analysis of interfacial interactions and reactivity between the components indicates that the EMAG will preferentially disperse in the PGA phase. Therefore, a two-step blending method was designed to change reaction kinetics of PGA and PBAT grafted EMAG chain, so that the EMAG would be dispersed at the interface of PGA and PBAT. The PBAT/EMAG mixtures were first prepared to in-situ form PBAT-g-EMAG copolymers which could reduce the interfacial tension between PBAT and EMAG. Next, the PGA was compounded with PBAT/EMAG, and the PGA was also attached to the EMAG chains to form interface-localized PGA-g-E-MAG-g-PBAT copolymers for better compatibilization efficiency.

3.2. Formation of copolymers during the mixing process

^{1}H NMR was performed to verify the formation of EMAG-g-PBAT copolymer during the preparation of PBAT/EMAG mixtures. The ^{1}H NMR spectra of PBAT/EMAG mixtures prepared at 190 °C and 230 °C and the sample after removal of unreacted PBAT from cyclohexane are
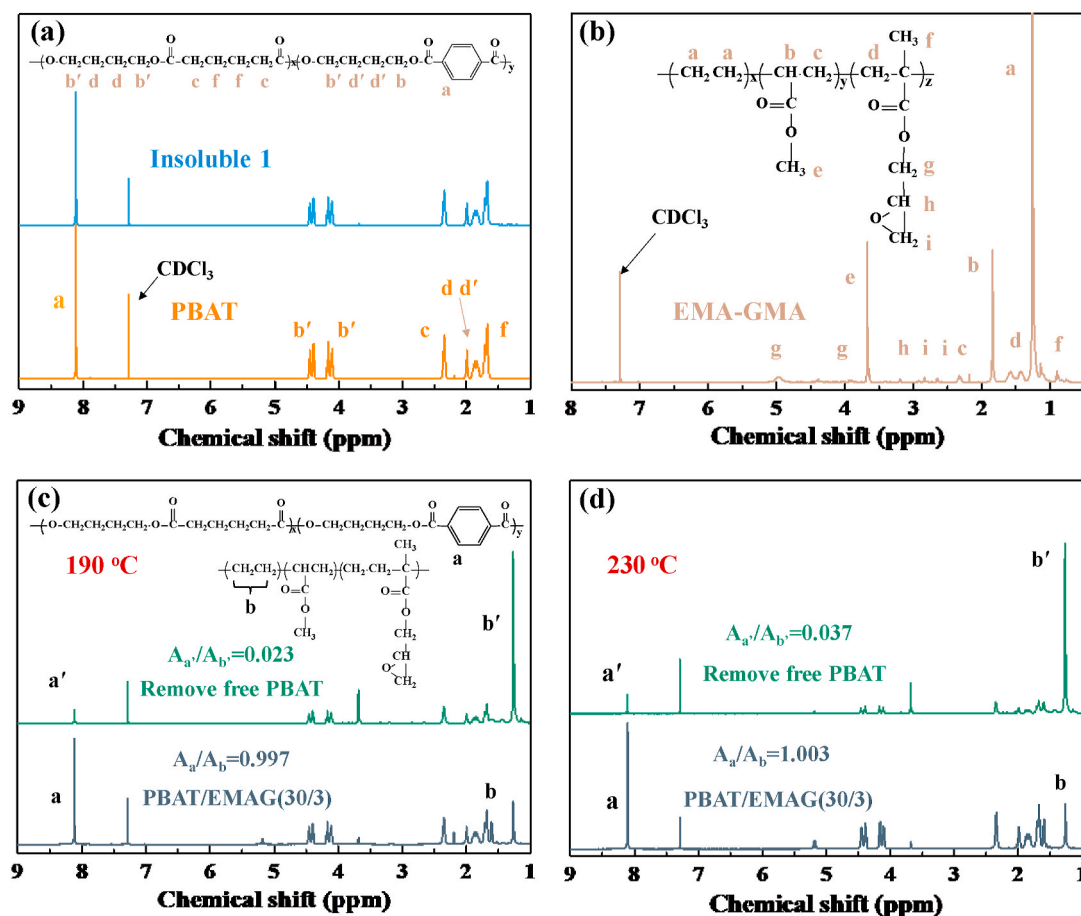

Fig. 2. ^{1}H NMR spectra for (a) pure PBAT and insoluble 1, (b) pure EMAG, (c–d) the PBAT/EMAG blend before and after removing the unreacted PBAT at 190 °C and 230 °C.
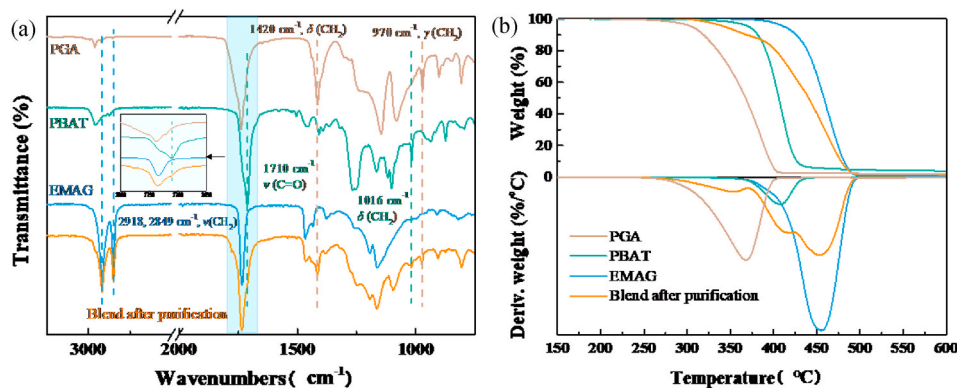
Fig. 3. (a) FT-IR spectra and TGA curves for of PGA, PBAT, EMAG and the G/(B/EG) blend after purification.

shown in Fig. 2c and d. The spectra of pure PBAT and EMAG are also given in Fig. 2a and b as references. The characteristic proton signals at 8.1 ppm and 1.3 ppm are assigned to the phenyl group in PBAT and methylene protons of ethylene units in EMAG, respectively. Fig. 2a demonstrates that the insoluble 1 (obtained from the separation procedure shown in Scheme 2) is unreacted PBAT without any EMAG components. After removal of the unreacted PBAT, the characteristic resonance peak at 8.1 ppm still existed, confirming that the formation of EMAG-g-PBAT copolymer (Fig. 2c and d). The grafting efficiency (GE) defined as the percentage mass fraction of reacted PBAT to the initial fed PBAT and the grafting degree (GD) defined as the weight ratio of the grafted PBAT in PBAT/EMAG after removing unreacted PBAT were measured by following equations:

$$GE = \frac{A'_a}{A'_b} \bigg/ \frac{A_a}{A_b} \times 100\%$$

$$GD = \frac{30 \times GE}{3 + 30 \times GE} \times 100\%$$

where A and A'_i are the areas of the resonance peak i before and after removing unreacted PBAT. 30 and 3 are the weight ratio of PBAT and EMAG of the PBAT/EMAG blend, respectively. The ^{1}H NMR results shows that the GE and GD of PBAT are 2.3%, 18.7% at 190 °C and 3.7%, 27% at 230 °C, respectively. The GD of PBAT during melt blending at 190 °C is lower than that at 230 °C, indicating an incomplete reaction

between epoxy groups of EMAG and PBAT at 190 °C. It is verified that PBAT successfully reacted with EMAG to form PBAT-g-EMAG copolymer during the first step melt-compounded at 190 °C and EMAG could continue react with PGA in the second melt-blending process.

In order to verify the formation of PGA-g-EMAG-g-PBAT copolymers in the second mixing step, the unreacted PGA and PBAT of blends were firstly removed by Hexafluoroisopropanol (HFIP), which is a good solvent of PGA and PBAT but poor solvent of EMAG. The molecular structure of purified samples was characterized by FT-IR (Fig. 3a). The characteristic absorption peaks at 2918 cm^{-1} and 1849 cm^{-1} are assigned to the stretching vibration of –CH$_2$ of the EMAG [49]. The absorption peaks at 1420 cm^{-1} and 970 cm^{-1} are bending and rocking vibration of –CH$_2$ of the grafted PGA, respectively [12]. The grafted PBAT is then confirmed by the peak at 1710 cm^{-1} corresponding to stretching vibration of carbonyl groups and the peak at 1016 cm^{-1} attributing to bending vibration of –CH$_2$ of the PBAT [50]. Moreover, thermogravimetric analysis (TGA) was also utilized to characterize the composition of the PGA-g-EMAG-g-PBAT copolymers. As shown in Fig. 3b, PGA, PBAT, EMAG only exhibit one decomposition peak, while the purified samples show three decomposition peaks corresponding to PGA, PBAT, and EMAG, respectively. All these results confirmed that PGA and PBAT are grafted onto the EMAG chains forming comb-like PGA-g-EMAG-g-PBAT copolymers. However, the accurate grafting degrees of PBAT and PGA is not obtained due to the overlapping of the decomposition temperature of these components.
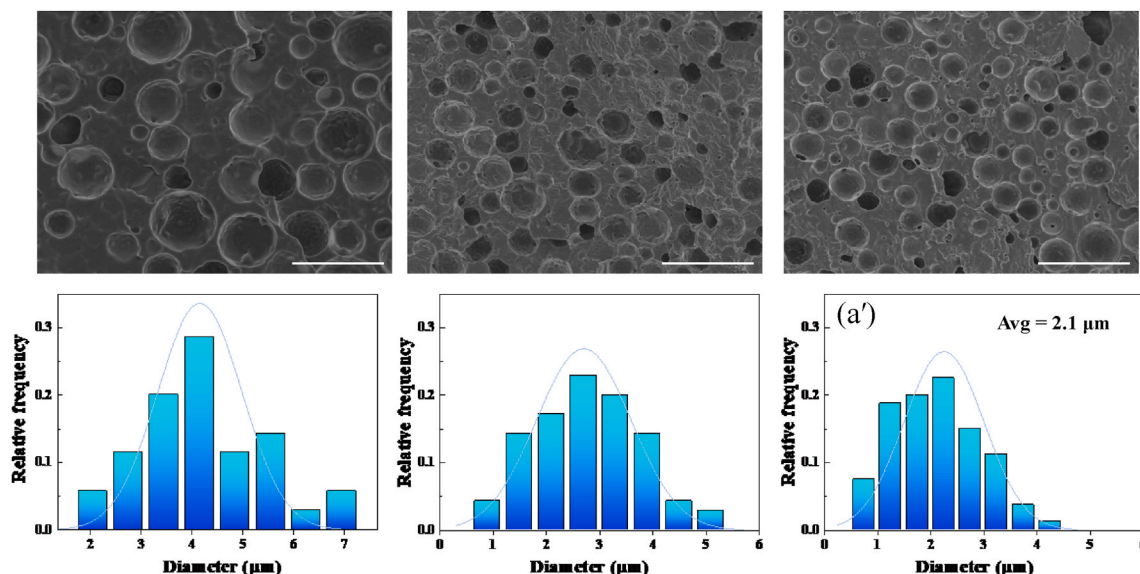

Fig. 4. SEM images and the size distribution of the dispersed phase of PBAT in blends (a)/(a′) G/B, (b)/(b′) G/B/EG1, (c)/(c′) G/(B/EG1).
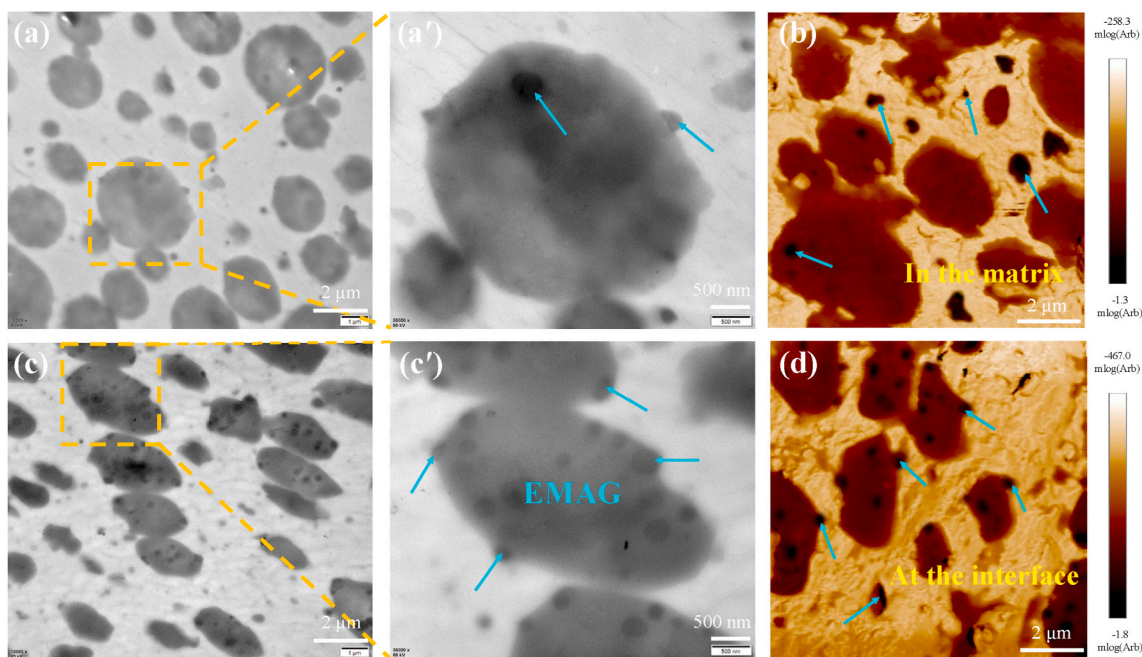
Fig. 5. TEM and AFM images of (a)/(a′)/(b) G/B/EG1, (c)/(c′)/(d) G/(B/EG1) blends.

3.3. Morphological evolution and compatibilization mechanisms of PGA/ PBAT blends

The SEM images of the cryo-fractured surface of G/B, G/B/EG1, and G/(B/EG1) blends are shown in Fig. 4. The PBAT and EMAG phases were extracted by chloroform to clearly distinguish the different phases. As expected, a typical sea-island structure is observed in all blends (i.e., the PBAT or EMAG droplets are distributed in PGA matrix). The average size of dispersed phase of the binary blend without compatibilizer is 4.3 μm (Fig. 4a), and it decreases evidently by adding 1 wt % EMAG into the
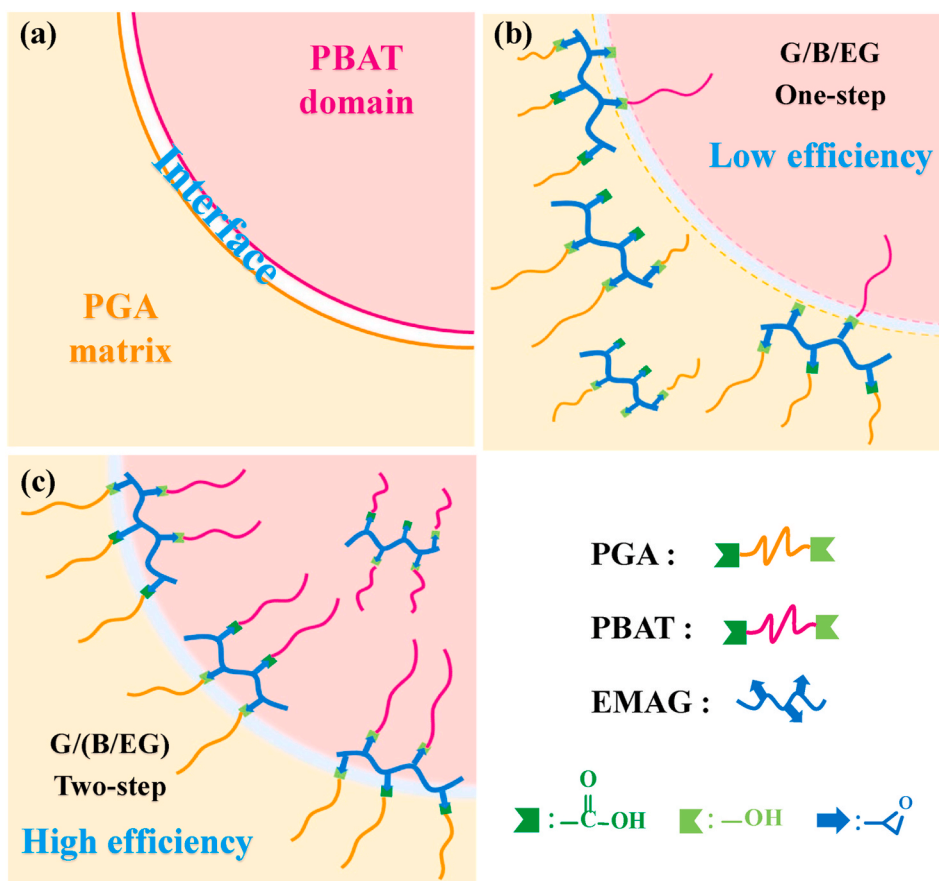

Fig. 6. Schematic illustration of the morphology and the compatibilization mechanisms of (a) G/B, (b) G/B/EG1, (c) G/(B/EG1) blends.
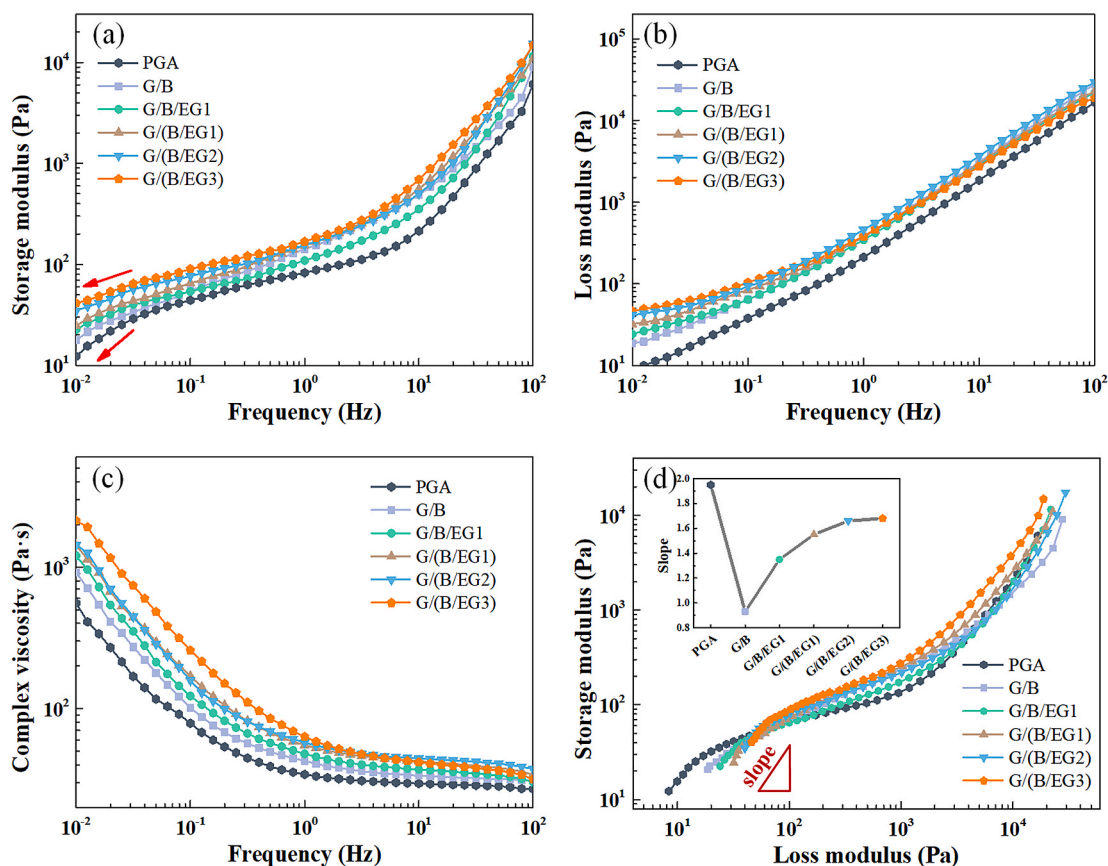
Fig. 7. Frequency dependence of dynamic viscoelastic properties of PGA, G/B, G/B/EG1 and G/(B/EG*x*) blends with different ratios of EMAG: (a) storage modulus; (b) loss modulus; (c) complex viscosity; (d) Han curves.

blend. Interestingly, the dispersed phase size of the G/(B/EG1) blend prepared via two-step melt blending is 2.1 μm (Fig. 4c), which is smaller than G/B/EG1 (2.8 μm, Fig. 4b) via one-step melt blending. Although the absolute value of reduction seems not so significant, it is 25% smaller already compared with the average diameter of the one-step mixing blends. The decrease in average size of the dispersed phase indicates a better compatibility between PBAT phase and PGA matrix. Due to the reactions of EMAG with PGA and PBAT, the compatibility in G/B/EG1 and G/(B/EG1) blends is better than for the G/B blend. But as mentioned before in the interactions and reactivity analysis, the EMAG preferentially disperses in PGA phase in G/B/EG1 blend and resulting in an inefficient compatibilization effect. In the contrast, in the G/(B/EG1) blend prepared by the two-step blending processes, EMAG will be located at the interface to form interface-localized PGA-g-EMAG-g-PBAT copolymers, which markedly improves the interfacial adhesion. Therefore, the compatibility between PBAT and PGA is further enhanced in G/(B/EG1) blend compared to the G/B/EG1.

To further confirm the state of dispersion of EMAG particles in ternary blends, the TEM and AFM micrographs of G/B/EG1 and G/(B/EG1) blends are shown in Fig. 5. In the AFM image, the light domains are the PGA matrix with high modulus, the brown domains represent the PBAT droplets with low modulus and the dark phase is classified as the EMAG. The TEM and AFM micrographs in Fig. 5a and b reveal that a large amount of EMAG (as marked by the blue arrows) is dispersed in the PGA matrix and few particles of EMAG are dispersed in PBAT phase or at the interface of PGA and PBAT in the G/B/EG1 blend, which is consistent with the previous prediction. It should be noticed that it is hard to distinguish EMAG located in the matrix and PBAT in the TEM image, so only a small amount of EMAG distributed in PBAT is observed in Fig. 5a, a′. Interestingly, a partial wetting formation in the G/(B/EG1) blend is exactly observed in Fig. 5c, c′. The EMAG and PBAT formed a "multiple

stacked structure" similar to that reported by Zhang et al. [51]. Multiple dispersed small droplets were found around the edge of a large particle. Fig. 5d clearly indicates that a lot of EMAG domains are localized at the interface between PGA and PBAT. It is worth noting that there is no obvious evidence of the agglomerated structures of EMAG phase in PGA matrix for the G/(B/EG1) blend.

Fig. 6 schematically illustrates the phase morphological evolution of G/B, G/B/EG1, and G/(B/EG1) blends. The EMAG is an efficient interfacial compatibilizer for PGA/PBAT blend. But the distribution of EMAG in G/B/EG1 blend and G/(B/EG1) blend is different, resulting in different compatibilization efficiency. The difference in distribution of EMAG is mainly attributed to the reactivity of EMAG with PGA and PBAT during the melting blending. During the one-step blending processes, most EMAG chains react with PGA and are fixed in the PGA matrix, so the compatibilization efficiency is poor. Corresponding, in the two-step blending processes, EMAG chains react with PBAT during the first melt blending of preparing PBAT/EMAG mixtures (as had been demonstrated in NMR result) and further react with PGA to form interface-localized PGA-g-EMAG-g-PBAT copolymers in the second step. The interface-localized copolymers notably enhanced the interfacial adhesion, resulting in high compatibilization efficiency.

3.4. Rheological characterization of compatibility and melt strength in blends

The dynamic rheological characterization is an important and sensitive method to evaluate the interfacial interactions, phase morphologies and melt-processability of polymer blends. Frequency dependence of dynamic rheological properties can give valuable information regarding phase interactions of multiphase polymeric systems. The changes of dispersion state and interfacial interactions by reactive
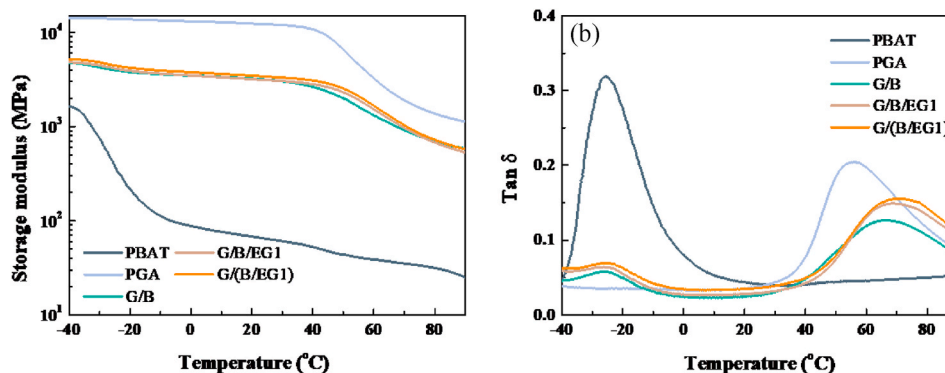
Fig. 8. Temperature dependence of (a) storage modulus and (b) damping factor for PGA, PBAT and their blends.

compatibilization are usually reflected at low frequency regions. Therefore, the analysis of rheology properties was further used to determine change of the interfacial interactions, compatibility and melt strength of the PGA/PBAT/EMAG ternary systems.

Fig. 7 presents the frequency dependence of (a) storage modulus (G′), loss modulus (G″) and (c) complex viscosity (η*) of neat PGA, G/B, G/B/EG1 and G/(B/EGx) blends with various EMAG content. The G′ and G″ refer to the ability to store and consume energy during the deformation process. According to modulus data in Fig. 7, all PGA/PBAT blends represent higher energy storage capacity than neat PGA, because PBAT possesses superior melt elasticity compared to PGA. The incorporation of EMAG further increases the G′ of blends, which is due to the increasement of the entanglement and interfacial adhesion caused by the reaction of EMAG with both PGA and PBAT chains. At low frequency region, the termination of the G/(B/EGx) blends curves are mostly independent of frequency and exhibit a plateau response. Such the nonterminal relaxation behavior arises from the entangled or network-like structures of copolymer domain formed by the addition of EMAG. It is noting that the plateau response of G/(B/EG1) blend is more obvious than that of G/B/EG1 because more copolymers are formed in the G/(B/EG1) blend. The complex viscosity data in Fig. 7b demonstrate that all the samples showed a strong shear-thinning tendency which might be a characteristic of PGA. In comparison with neat PGA, the blends reveal much higher complex viscosity over the entire frequency range and the viscosity difference of them becomes more obvious as the decrease of the frequency. Similarly, the complex viscosity of G/(B/EG1) blend is higher than that of G/B/EG1 blend. The complex viscosity gradually enhanced with the increase of EMAG content in G/(B/EG) blends. The higher complex viscosity is attributed to the in-situ formation of PGA-g-EMAG-g-PBAT copolymers, which enhances the interfacial interaction and chain entanglement between PGA and PBAT. It is worth noting that the rheological behavior of pure PGA differs from that of typical linear polymers, i.e., a wide shoulder in G′ is observed and the viscosity seems go to infinity as frequency decreases. The relatively low testing temperature (230 °C) could generate fine residual crystals in the melt, as indicated by the so-called self-nucleation phenomenon, as shown in Fig. S2. Although the PGA used in this work is a liner polymer, the residual crystals in the melt as physical crosslinking points would lead to locally network or branching structures which should be responsible for the particular rheological behavior of the PGA.

It is well documented that the Han plots could be used to investigate the compatibility of multiphase polymers systems [52,53]. According to Fig. 7d, the logarithmic slope of the G′ versus G″ plots of neat PGA is about 2 at the end of the low frequency region. By contrast, the slope of low frequency of G/B blend curve deviates obviously, suggesting the poor compatibility between PGA and PBAT phase. A better compatibility can be indicated when the slope of low frequency of blends is close to that of PGA. The addition of 1% EMAG enhanced the compatibility of PGA and PBAT. The slope the curve of the G/(B/EG1) blend prepared by

Table 3
Thermal properties of PGA, PBAT, and their blends.

samples	$T_{g,PBAT}$ (°C)	$T_{g,PGA}$ (°C)
Neat PGA	/	55.9
Neat PBAT	−26.3	/
G/B	−25.2	65.5
G/B/EG1	−24.4	68.7
G/(B/EG1)	−23.8	71.2

two-step blending process is further increased, which indicates the further improvement of the compatibility. As an increase in the EMAG content, both G′ and G″ of blends improved. Meanwhile, the slope of the end of the low frequency was getting close to that of neat PGA, which indicates the improvement in compatibility. With the EMAG content up to 3%, the change of slope is not obvious, probably owing to the saturated interfacial interactions.

In conclusion, the dynamic viscoelastic properties show that EMAG had great influence on the rheological behavior of PGA/PBAT/EMAG blends at low frequency regions. The PGA-g-EMAG-g-PBAT copolymers formed by EMAG reacting with PGA and PBAT could improve the interaction between PBAT particles and surrounding PGA matrix, thus affecting the low-frequency rheological behavior. The rheological results confirm that more PGA-g-EMAG-g-PBAT copolymers are obtained and causing better compatibilization efficiency in the G/(B/EG) blends prepared by a two-step blending process compared to the G/B/E blends, which is in accordance with morphological results. In addition, the copolymers enhance the entanglement density of the PGA/PBAT/EMAG blends, which cause restrictions for flow and slippage under shear deformation of macromolecular chains, thereby the melt viscosity and elasticity are increased significantly. The enhancement of melt strength is of great importance for PGA because the low melt strength is one of the drawbacks in limiting its processability.

3.5. Dynamic mechanical properties

Dynamic thermomechanical analysis (DMA) was applied to examine the interfacial interactions between phases after adding EMAG. The storage modulus (G′) and damping factor (tan δ) for PGA, PBAT, and PGA/PBAT/EMAG blends from −40 °C to 90 °C are shown in Fig. 8. The G′ is associated with the elastic response of materials, and the tan δ is related to the occurrence of chain relaxations. Table 3 summarizes the glass transition temperature (T_g) corresponding to tan δ peak of PGA, PBAT and PGA/PBAT/EMAG blends. The increase of T_g after blending with EMAG might be resulted from the enhanced crystallinity of PGA (Table S1) and the formation of grafting structures. A higher crystallinity could lead to closer packing of molecular chains, thus reducing the mobility of chain segments [54,55]. Compared to the G/B/EG1 blend, the T_g of PBAT and PGA is further increased while the crystallinity of
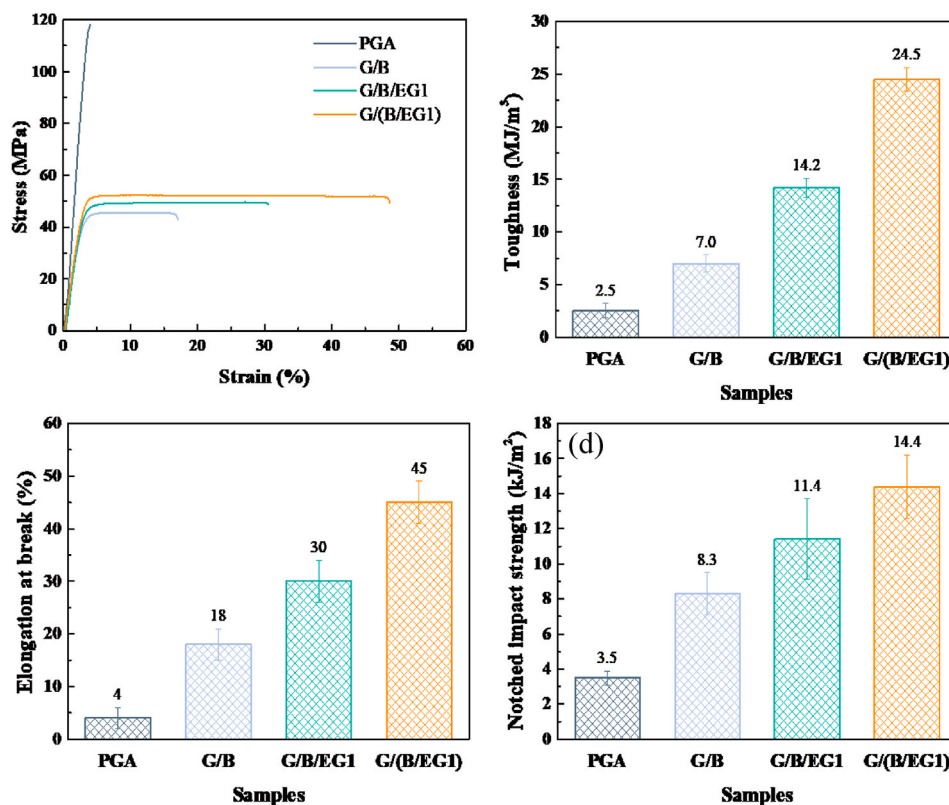
Fig. 9. (a) Stress-strain curves, (b) toughness, (c) elongation at break and (d) notched impact strength of PGA, G/B, G/B/EG1, and G/(B/EG1) blends.

PGA is decreased (Table S1) in the G/(B/EG1) blend prepared by the two-step blending process. It is suggested that more graft copolymers were formed in the G/(B/EG1) blend obstructing the movement of chain segments. These results indicates that the EMAG exhibit a better compatibilization efficiency in the G/(B/EG1) blend, which is consistent with the earlier statement.

3.6. Mechanical properties and tensile-fractured morphology

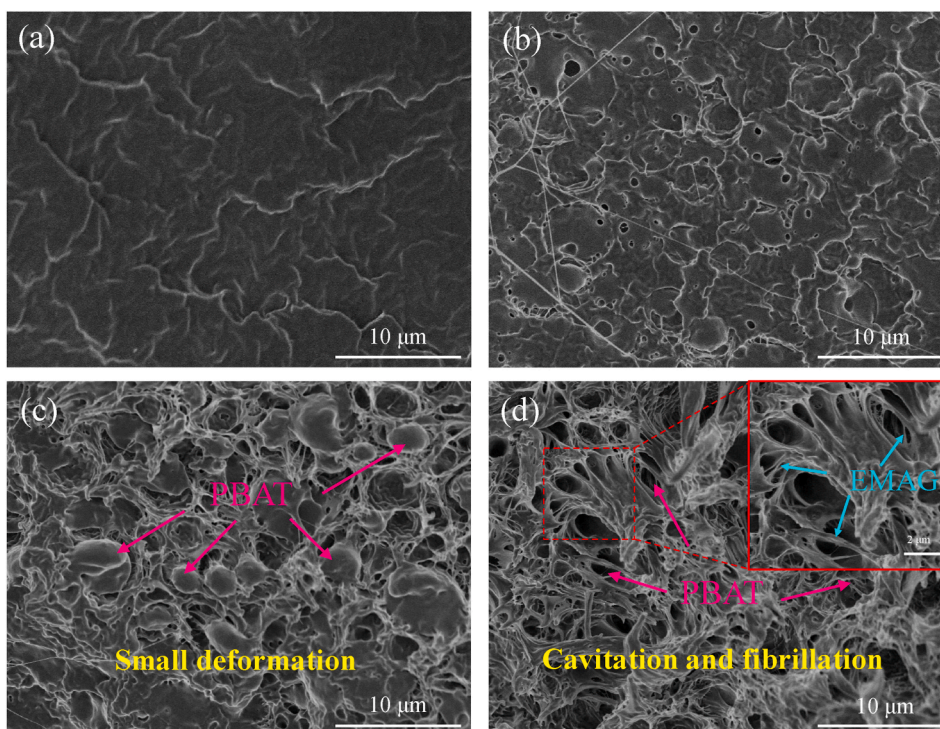To examine the effect of compatibility and interfacial interaction

Fig. 10. SEM images for tensile-fractured surfaces of (a) PGA, (b) G/B, (c) G/B/EG1, (d) G/(B/EG1).
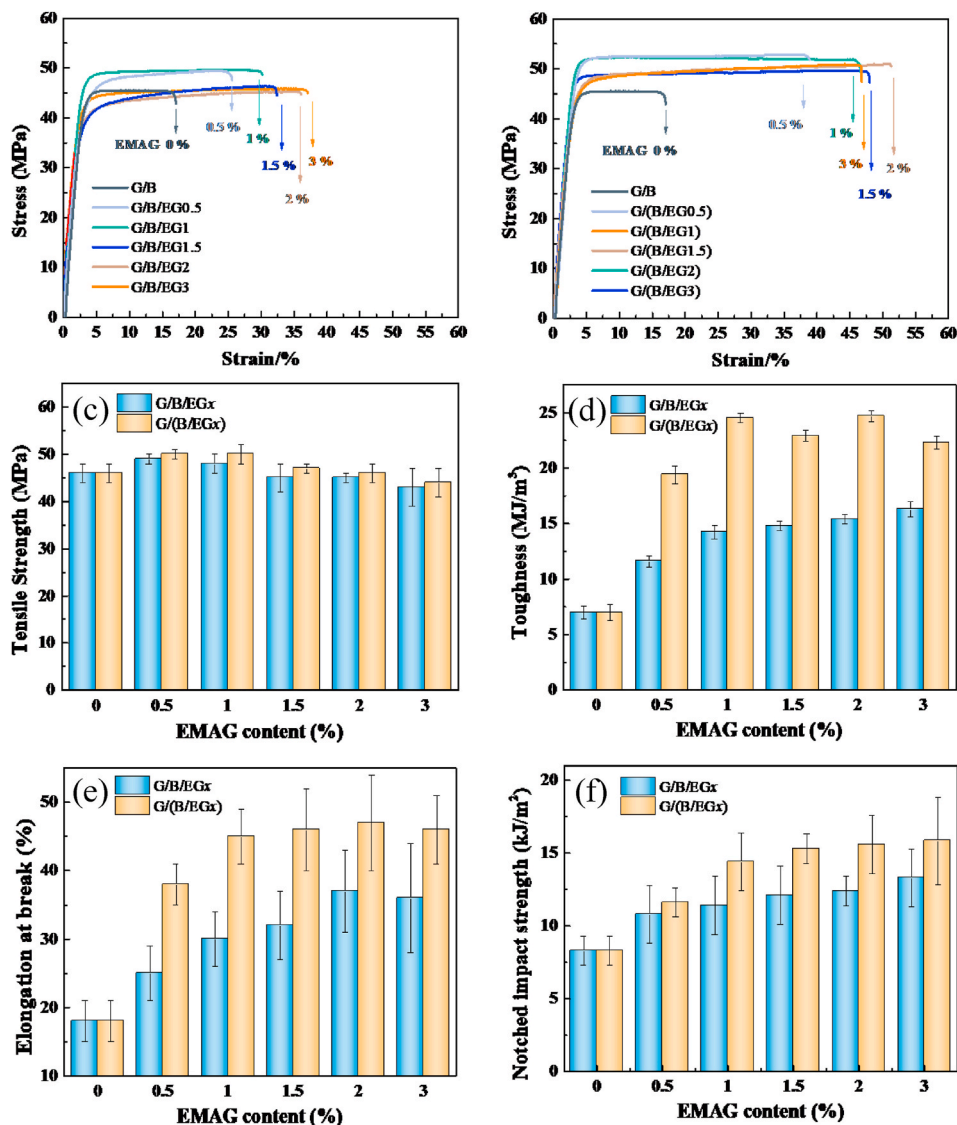
Fig. 11. Representative stress–strain curves of (a) G/B/EGx blends and (b) G/(B/EGx) blends. (c)toughness, (d) tensile strength, (e)elongation at break and (f) notched impact strength of G/B/EG and G/(B/EG) blends as a function of EMAG weight content.

between PGA matrix and PBAT phase on the mechanical response of PGA/PBAT/EMAG blends, Fig. 9 presents the tensile and impact properties of blends. Neat PGA behaves in completely brittle fracture with high tensile strength (≈117 MPa), low elongation at break (≈4.8%) and notched impact strength (3.5 kJ/m^2). When 30 wt % PBAT was incorporated into PGA, the mode of failure change from brittle to ductile. The elongation at break of the G/B blend is increased to 18%. But due to the poor interfacial interactions between PGA matrix and PBAT phase, the PBAT is debonded from the matrix easily and cause premature fracture of the material at relatively low stress or strain, which result in decreased strength/stress and inferior toughening effect. With the addition of EMAG, the elongation at break and impact strength of G/B/EG1 blend increase to 30% and 11.4 ± 2.3 kJ/m^2. It is interesting to note that the mechanical properties of G/(B/EG1) blend are further improved compared to the G/B/EG1 blend. The elongation at break of the G/(B/EG1) blend reaches $45 \pm 4\%$, which is 1100% and 150% higher than that of neat PGA and G/B/EG1 blend, respectively. The notched impact strength of G/(B/EG1) is also elevated to 14.4 ± 1.6 kJ/m^2, which is higher than that of other samples. The improvement in the strength and toughness of the G/(B/EG1) blend over G/B/EG1 blend is mainly attributed to further improvement of the interfacial adhesion, molecular

chain entanglement and decrease of the PBAT particle size by the formation of interface-localized PGA-g-EMAG-g-PBAT copolymers. Moreover, the mechanical properties of G/(B/EG1) blends prepared by mixing PBAT with EMAG at different temperatures are shown in Fig. S3. It is demonstrated that the preparation of PBAT/EMAG mixture at high temperature shows negative effects on the mechanical properties of G/(B/EG1) blends. It can be explained by that the PBAT consume more epoxy groups by reacting with EMAG at high temperature (which is confirmed by NMR results), resulting in a weaker reaction with PGA, thus the compatibilization is reduced.

The better interfacial adhesion causes the more efficient stress transfer from PGA matrix to PBAT phase. It is verified by SEM observation of the tensile-fractured surfaces of the materials and the micrographs are presented in Fig. 10. Neat PGA display a smooth and featureless surface with no deformation, suggesting a typical brittle fracture characteristic (Fig. 10a). When blending with 30% of PBAT, the fracture surface becomes rough, some voids and filaments are observed (Fig. 10b). In comparison to the binary blend, the 1% EMAG-containing blend prepared by one-step blending show a rougher fracture surface, and the plastic deformation and some fibrils are clearly observed (Fig. 10c), which is accordance with a moderate enhancement of
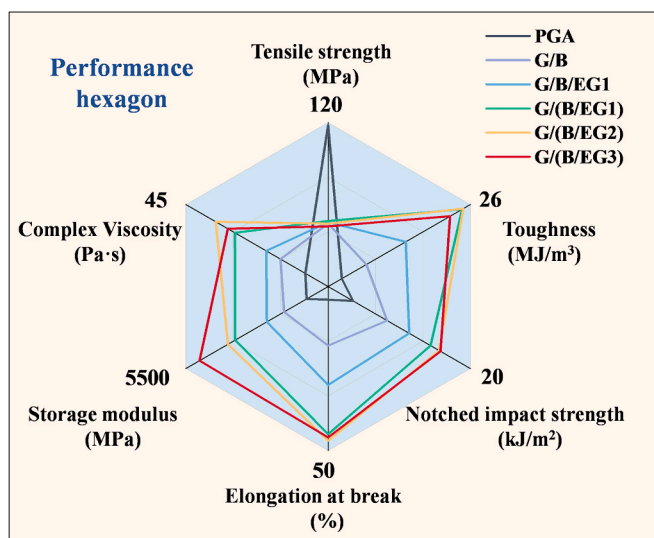
Fig. 12. Comparison of the comprehensive performance (in terms of tensile strength, toughness, impact strength, elongation at break, storage modulus and viscosity) between PGA, G/B, G/B/EG1, G/(B/EGx) blends.

toughness (Fig. 9). However, the deformation of PBAT particles (as marked by the blue arrows) is still insignificant due to the unsatisfactory improvement in interfacial adhesion, indicating an inefficient stress transfer from PGA to the PBAT phase. As expected, the more and longer fibril threads, significant plastic deformation and many voids in the case of the G/(B/EG1) blend are further noticed (Fig. 10d). Furthermore, Fig. 10d illustrates an obvious deformation of PBAT particles and elongated fibrils of EMAG (as marked by the yellow arrows) between PBAT phase and PGA matrix. It shows that EMAG acts as a bridge between PBAT and PGA to provide strong interfacial bonding. Great stress transfer from PGA matrix to PBAT phase causing fibrillation and cavitation of the PBAT, thus promoting the shear yield of matrix. As evidenced by the date in Fig. 10 and the morphological observations in Figs. 4 and 5, the dispersion of PBAT in the G/(B/EG1) blend is finer and more homogeneous, the interfacial bonding between the PBAT and surrounding matrix is stronger, which could trigger more regions to participate in the deformation process.

3.7. Effect of EMAG content on the performance of blends

The effect of interfacial adhesion development induced by EMAG content and processing method in the PGA/PBAT/EMAG (70-30-x) blends on mechanical response under the notched impact and tensile tests was investigated. Fig. 11 depicts the mechanical properties of G/B, G/B/EG and G/(B/EG) blends with different EMAG contents. The typical stress−strain curves of blends prepared by one-step and two-step blending process are presented in Fig. 11a and b, respectively. As shown in the figures, the tensile strength and the elongation at break of the G/B blends are 46 ± 2 MPa and $18 \pm 3\%$. As the content of EMAG increases from 0.5% to 2%, the elongation at break of the G/B/EGx blends increases from $25 \pm 4\%$ to $38 \pm 5\%$, and then decreases slightly at 3% of EMAG. The toughness and notched impact strength of the resulted material increases monotonically while the EMAG content increases. In contrast, with increasing EMAG content, the tensile strength of the blends increases initially, followed by a decrease, which is probably attributed to the variation in the crystallinity of the blends. The variation of crystallinity of the blends is consistent with the strength (see Fig. S4 and Table S1). Fig. 11 c-f displays the toughness, tensile strength, elongation at break and notched impact strength of PGA/PBAT/EMAG blends prepared by one-step and two-step processing. It obviously indicates that mechanical performance of G/(B/EGx) blends is changed

with EMAG concentration in the same tends as that of the G/B/EGx blends. Intriguingly, the G/(B/EGx) blends show a simultaneously enhancement in the tensile strength and toughness under the same EMAG content compared to the G/B/EGx blends. In addition, the toughness of G/(B/EG) decreases as the EMAG content increases to 3%. This is because the compatibilization effect of EMAG worsens and the tensile toughness decreases consequently when the EMAG content reaches an optimum level, which is consistent with the dynamic rheological result.

Based on the results of this work, Fig. 12 summarizes the comprehensive performance of PGA, PGA/PBAT and PGA/PBAT/EMAG blends. In order to estimate the melt strength under the processing conditions, the storage modulus and complex viscosity date at 50.1 Hz (which is closest the average shear rate of Haake mixing with a rotor speed of 60 rpm [18,56]) are compared. It has to be remarked that Cox-Merz rule was not applied in this work since it mainly fits homogeneous melt system, thus the complex viscosity was not converted into shear viscosity. Obviously, the PGA-based blends with excellent ductility, toughness and melt strength were prepared by two-step melt reactive blending, which utilized PBAT as flexible polymer and EMAG as compatibilizer. The in-situ formation of interface-localized PGA-g-E-MAG-g-PBAT copolymers enhance the compatibility, interfacial interactions and chain entanglement between PGA and PBAT, thereby substantially enhancing the mechanical performance and melt strength of the blends.

4. Conclusions

In this work, bio-compostable and superior toughened PGA/PBAT blends with enhanced melt strength have been successfully prepared by reactive blending using EMAG as compatibilizer. Owing to the difference in interfacial tension and reactivity among EAMG, PGA and PBAT, the EMAG prefers to be encapsulated in the PGA matrix. Thus, a feasible and effective two-step method was designed to control dispersion state of EMAG in PGA/PBAT blend and improve the interfacial interactions between PGA and PBAT. EMAG was first blended with PBAT at 190 °C and then compounded with PGA, so that EMAG is located at the interface to in-situ formed interface-localized PGA-g-EMAG-g-PBAT copolymers. The copolymers markedly enhance the interfacial adhesion and compatibility between PGA and PBAT, which is evidenced by phase morphological, dynamic rheological and DMA. Meanwhile, the copolymers also act as a bridge to transfer more effective energy from PGA matrix to the PBAT phase when the blends are subjected to tensile or impact stress, resulting in a high toughening effect. The dynamic rheological and DMA results confirm the melt strength and glass transition of PGA are improved by the formation of copolymers. As a consequence, excellent mechanical properties are obtained as PGA/(PBAT/EMAG) blend with only 1 wt % EMAG content. The elongation at break and the notched impact strength reached $45 \pm 4\%$ (1100% and 150% times higher than neat PGA and GB/EG1) and 14.4 ± 1.6 kJ/m^2, respectively. It is an excellent improvement for PGA materials. Besides the blend also possesses a good tensile strength (>50 MPa). Moreover, the dynamic rheological confirm that the viscosities and storage modulus of PGA/(PBAT/EMAG) blends are greatly enhanced compared with PGA. The present work provides a novel method to fabricate high-performance PGA-based blends and a promising way to expand the application field of PGA materials.

Supporting Information

Characterization details; Mechanical properties of G/(B/EG1) blends prepared by blending PBAT/EMAG mixtures at different temperatures; DSC curves and thermal parameters of PGA, PBAT, G/B and G/(B/EGx) blends with various EMAG content.

Author statement

Deyu Niu: Writing-original draft, Formal analysis, Data collection and analysis. W. Pengwu Xu: Investigation, Formal analysis, Writing-review & editing. Zhaoyang Sun and Weijun Yang: Investigation, Formal analysis. Weifu Dong and Yang Ji: Writing-original draft. Tianxi Liu and Mingliang Du: Data collection and analysis, Writing-original draft preparation, P. Lemstra: Investigation, Formal analysis, Writing-review & editing. P. Ma: Conceptualization, Supervision, Writing-review & editing.

Declaration of competing interest

The authors declare that they have no known competing financial interests or personal relationships that could have appeared to influence the work reported in this paper.

Acknowledgments

Appendix A. Supplementary data

Supplementary data to this article can be found online at https://doi.org/10.1016/j.polymer.2021.124269.

References

[1] Z. Wang, M.S. Ganewatta, C. Tang, Sustainable polymers from biomass: bridging chemistry with materials and processing, Prog. Polym. Sci. 101 (2020) 101197, https://doi.org/10.1016/j.progpolymsci.2019.101197.

[2] J.W. Rhim, H.M. Park, C.S. Ha, Bio-nanocomposites for food packaging applications, Prog. Polym. Sci. 38 (2013) 1629–1652, https://doi.org/10.1016/j.progpolymsci.2013.05.008.

[3] H. Kargarzadeh, M. Mariano, J. Huang, N. Lin, I. Ahmad, A. Dufresne, S. Thomas, Recent developments on nanocellulose reinforced polymer nanocomposites: a review, Polymer 132 (2017) 368–393, https://doi.org/10.1016/j.polymer.2017.09.043.

[4] M. Maroufkhani, A.A. Katbab, H. Bizhani, J. Zhang, Toward morphology development and impact strength of Co-continuous supertough dynamically vulcanized rubber toughened PLA blends: effect of sulfur content, Polymer 217 (2021) 123439, https://doi.org/10.1016/j.polymer.2021.123439.

[5] K. Yamane, H. Sato, Y. Ichikawa, K. Sunagawa, Y. Shigaki, Development of an industrial production technology for high-molecular-weight polyglycolic acid, Polym. J. 46 (2014) 769–775, https://doi.org/10.1038/pj.2014.69.

[6] P.K. Samantaray, A. Little, D.M. Haddleton, T. McNally, B. Tan, Z. Sun, W. Huang, Y. Ji, C. Wan, Poly(glycolic acid) (PGA): a versatile building block expanding high performance and sustainable bioplastic applications, Green Chem. 22 (2020) 4055–4081, https://doi.org/10.1039/d0gc01394c.

[7] L.K. Li, L.L. Shi, P.H. Hong, T.W. Tan, Z.J. Li, Metabolic engineering of Escherichia coli for the production of glyoxylate from xylose, Biochem. Eng. J. 129 (2018) 113–118, https://doi.org/10.1016/j.bej.2017.11.002.

[8] X. Lu, Y. Yao, Y. Yang, Z. Zhang, J. Gu, L. Mojovic, Z. Knezevic-Jugovic, F. Baganz, G. Lye, J. Shi, J. Hao, Ethylene glycol and glycolic acid production by wild-type Escherichia coli, Biotechnol. Appl. Biochem. (2020) 1–12, https://doi.org/10.1002/bab.1987.

[9] E. Swider, O. Koshkina, J. Tel, L.J. Cruz, I.J.M. de Vries, M. Srinivas, Customizing poly(lactic-co-glycolic acid) particles for biomedical applications, Acta Biomater. 73 (2018) 38–51, https://doi.org/10.1016/j.actbio.2018.04.006.

[10] M. Ansari, S. Moradi, M. Shahlaei, A molecular dynamics simulation study on the mechanism of loading of gemcitabine and camptothecin in poly lactic-co-glycolic acid as a nano drug delivery system, J. Mol. Liq. 269 (2018) 110–118, https://doi.org/10.1016/j.molliq.2018.08.032.

[11] Y. Liu, T. Nelson, B. Cromeens, T. Rager, J. Lannutti, J. Johnson, G.E. Besner, HB-EGF embedded in PGA/PLLA scaffolds via subcritical CO2 augments the production of tissue engineered intestine, Biomaterials 103 (2016) 150–159, https://doi.org/10.1016/j.biomaterials.2016.06.039.

[12] C. Yu, J. Bao, Q. Xie, G. Shan, Y. Bao, P. Pan, Crystallization behavior and crystalline structural changes of poly(glycolic acid) investigated: via temperature-variable WAXD and FTIR analysis, CrystEngComm 18 (2016) 7894–7902, https://doi.org/10.1039/c6ce01623e.

[13] H. Liu, W. Song, F. Chen, L. Guo, J. Zhang, Interaction of microstructure and interfacial adhesion on impact performance of polylactide (PLA) ternary blends, Macromolecules 44 (2011) 1513–1522, https://doi.org/10.1021/ma1026934.

[14] J. Zhao, H. Pan, H. Yang, J. Bian, H. Zhang, G. Gao, L. Dong, Study on miscibility, thermal properties, degradation behaviors, and toughening mechanism of poly (lactic acid)/poly (ethylene-butylacrylate-glycidyl methacrylate) blends, Int. J. Biol. Macromol. 143 (2020) 443–452, https://doi.org/10.1016/j.ijbiomac.2019.11.226.

[15] Z. Cao, H. Pan, Y. Chen, L. Han, J. Bian, H. Zhang, L. Dong, Y. Yang, Ductile and biodegradable poly (lactic acid) matrix film with layered structure, Int. J. Biol. Macromol. 137 (2019) 1141–1152, https://doi.org/10.1016/j.ijbiomac.2019.07.047.

[16] Y. Liu, L. Cao, D. Yuan, Y. Chen, Design of super-tough co-continuous PLA/NR/SiO2 TPVs with balanced stiffness-toughness based on reinforced rubber and interfacial compatibilization, Compos. Sci. Technol. 165 (2018) 231–239, https://doi.org/10.1016/j.compscitech.2018.07.005.

[17] M.M. Mazidi, R. Berahman, A. Edalat, Phase morphology, fracture toughness and failure mechanisms in super-toughened PLA/PB-g-SAN/PMMA ternary blends: a quantitative analysis of crack resistance, Polym. Test. 67 (2018) 380–391, https://doi.org/10.1016/j.polymertesting.2018.03.028.

[18] B. Wu, Q. Zeng, D. Niu, W. Yang, W. Dong, M. Chen, P. Ma, Design of supertoughened and heat-resistant PLLA/elastomer blends by controlling the distribution of stereocomplex crystallites and the morphology, Macromolecules 52 (2019) 1092–1103, https://doi.org/10.1021/acs.macromol.8b02262.

[19] D. Huang, Y. Ding, H. Jiang, S. Sun, Z. Ma, K. Zhang, L. Pan, Y. Li, Functionalized elastomeric ionomers used as effective toughening agents for poly(lactic acid): enhancement in interfacial adhesion and mechanical performance, ACS Sustain. Chem. Eng. 8 (2020) 573–585, https://doi.org/10.1021/acssuschemeng.9b06123.

[20] J. Huang, J. Fan, L. Cao, C. Xu, Y. Chen, A novel strategy to construct co-continuous PLA/NBR thermoplastic vulcanizates: metal-ligand coordination-induced dynamic vulcanization, balanced stiffness-toughness and shape memory effect, Chem. Eng. J. 385 (2020) 123828, https://doi.org/10.1016/j.cej.2019.123828.

[21] J. Andrzejewski, J. Cheng, A. Anstey, A.K. Mohanty, M. Misra, Development of toughened blends of poly(lactic acid) and poly(butylene adipate- co-terephthalate) for 3D printing applications: compatibilization methods and material performance evaluation, ACS Sustain. Chem. Eng. 8 (2020) 6576–6589, https://doi.org/10.1021/acssuschemeng.9b04925.

[22] W. Phetwarotai, M. Zawong, N. Phusunti, D. Aht-Ong, Toughening and thermal characteristics of plasticized polylactide and poly(butylene adipate-co-terephthalate) blend films: influence of compatibilization, Int. J. Biol. Macromol. 183 (2021) 346–357, https://doi.org/10.1016/j.ijbiomac.2021.04.172.

[23] H. Pan, Z. Li, J. Yang, X. Li, X. Ai, Y. Hao, H. Zhang, L. Dong, The effect of MDI on the structure and mechanical properties of poly(lactic acid) and poly(butylene adipate-co-butylene terephthalate) blends, RSC Adv. 8 (2018) 4610–4623, https://doi.org/10.1039/c7ra10745e.

[24] Y. Ding, W. Feng, B. Lu, P. Wang, G. Wang, J. Ji, PLA-PEG-PLA tri-block copolymers: effective compatibilizers for promotion of the interfacial structure and mechanical properties of PLA/PBAT blends, Polymer 146 (2018) 179–187, https://doi.org/10.1016/j.polymer.2018.05.037.

[25] T.H. Zhao, W.Q. Yuan, Y.D. Li, Y.X. Weng, J.B. Zeng, Relating chemical structure to toughness via morphology control in fully sustainable sebacic acid cured epoxidized soybean oil toughened polylactide blends, Macromolecules 51 (2018) 2027–2037, https://doi.org/10.1021/acs.macromol.8b00103.

[26] J. Huang, L. Cao, D. Yuan, Y. Chen, Design of novel self-healing thermoplastic vulcanizates utilizing thermal/magnetic/light-triggered shape memory effects, ACS Appl. Mater. Interfaces 10 (2018) 40996–41002, https://doi.org/10.1021/acsami.8b18212.

[27] B. Xue, H.Z. He, Z.X. Huang, Z. Zhu, F. Xue, S. Liu, B. Liu, Fabrication of super-tough ternary blends by melt compounding of poly(lactic acid) with poly(butylene succinate) and ethylene-methyl acrylate-glycidyl methacrylate, Compos. B Eng. 172 (2019) 743–749, https://doi.org/10.1016/j.compositesb.2019.05.098.

[28] W. Yang, Y. Weng, D. Puglia, G. Qi, W. Dong, J.M. Kenny, P. Ma, Poly(lactic acid)/lignin films with enhanced toughness and anti-oxidation performance for active food packaging, Int. J. Biol. Macromol. 144 (2020) 102–110, https://doi.org/10.1016/j.ijbiomac.2019.12.085.

[29] P. Ma, P. Xu, Y. Zhai, W. Dong, Y. Zhang, M. Chen, Biobased poly(lactide)/ethylene-co-vinyl acetate thermoplastic vulcanizates: morphology evolution, superior properties, and partial degradability, ACS Sustain. Chem. Eng. 3 (2015) 2211–2219, https://doi.org/10.1021/acssuschemeng.5b00462.

[30] M. Nishida, H. Ichihara, H. Watanabe, N. Fukuda, H. Ito, Improvement of dynamic tensile properties of Poly(lactic acid)/Poly(butylene adipate-co-terephthalate) polymer alloys using a crosslinking agent and observation of fracture surfaces, Int. J. Impact Eng. 79 (2015) 117–125, https://doi.org/10.1016/j.ijimpeng.2014.11.010.

[31] W. Dong, B. Zou, P. Ma, W. Liu, X. Zhou, D. Shi, Z. Ni, M. Chen, Influence of phthalic anhydride and bioxazoline on the mechanical and morphological properties of biodegradable poly(lactic acid)/poly[(butylene adipate)-co-terephthalate] blends, Polym. Int. 62 (2013) 1783–1790, https://doi.org/10.1002/pi.4568.

[32] H. Liu, N. Chen, P. Shan, P. Song, X. Liu, J. Chen, Toward fully bio-based and supertough PLA blends via in situ formation of cross-linked biopolyamide continuity network, Macromolecules 52 (2019) 8415–8429, https://doi.org/10.1021/acs.macromol.9b01398.

[33] R. Al-Itry, K. Lamnawar, A. Maazouz, Improvement of thermal stability, rheological and mechanical properties of PLA, PBAT and their blends by reactive

extrusion with functionalized epoxy, Polym. Degrad. Stabil. 97 (2012) 1898–1914, https://doi.org/10.1016/j.polymdegradstab.2012.06.028.

[34] S. Deng, H. Bai, Z. Liu, Q. Zhang, Q. Fu, Toward supertough and heat-resistant stereocomplex-type polylactide/elastomer blends with impressive melt stability via in situ formation of graft copolymer during one-pot reactive melt blending, Macromolecules 52 (2019) 1718–1730, https://doi.org/10.1021/acs.macromol.8b02626.

[35] S. Jia, Y. Chen, J. Bian, H. Pan, X. Wang, L. Zhao, L. Han, H. Zhang, L. Dong, H. Zhang, Preparation and properties of poly(L-lactic acid) blends with excellent low-temperature toughness by blending acrylic ester based impact resistance agent, Int. J. Biol. Macromol. 183 (2021) 1871–1880, https://doi.org/10.1016/j.ijbiomac.2021.05.177.

[36] X. Wang, S. Peng, H. Chen, X. Yu, X. Zhao, Mechanical properties, rheological behaviors, and phase morphologies of high-toughness PLA/PBAT blends by in-situ reactive compatibilization, Compos. B Eng. 173 (2019) 107028, https://doi.org/10.1016/j.compositesb.2019.107028.

[37] B.P. Chang, A.K. Mohanty, M. Misra, Tuning the compatibility to achieve toughened biobased poly(lactic acid)/poly(butylene terephthalate) blends, RSC Adv. 8 (2018) 27709–27724, https://doi.org/10.1039/c8ra05161e.

[38] N. Virgilio, C. Marc-Aurèle, B.D. Favis, Novel self-assembling close-packed droplet array at the interface in ternary polymer blends, Macromolecules 42 (2009) 3405–3416, https://doi.org/10.1021/ma802544q.

[39] A.M. Zolali, B.D. Favis, Toughening of cocontinuous polylactide/polyethylene blends via an interfacially percolated intermediate phase, Macromolecules 51 (2018) 3572–3581, https://doi.org/10.1021/acs.macromol.8b00464.

[40] B. Wei, Q. Lin, X. Zheng, X. Gu, L. Zhao, J. Li, Y. Li, Reactive splicing compatibilization of immiscible polymer blends: compatibilizer synthesis in the melt state and compatibilizer architecture effects, Polymer 185 (2019) 121952, https://doi.org/10.1016/j.polymer.2019.121952.

[41] V.G. Papadakis, Estimation of surface free energy of polymers, J. Appl. Polym. Sci. 13 (1969) 1741–1747.

[42] C. Chen, Y. Tian, F. Li, H. Hu, K. Wang, Z. Kong, W. Bin Ying, R. Zhang, J. Zhu, Toughening polylactic acid by a biobased poly(butylene 2,5-Furandicarboxylate)-b-Poly(Ethylene glycol) copolymer: balanced mechanical properties and potential biodegradability, Biomacromolecules 22 (2021) 374–385, https://doi.org/10.1021/acs.biomac.0c01236.

[43] V.H.W.S.Y. Hobbs, M.E. Dekkers, Effect of interfacial forces on polymer blend morphologies, Polymer 29 (1988) 1598–1602, https://doi.org/10.1016/0032-3861(88)90269-8.

[44] T.S. Valera, A.T. Morita, N.R. Demarquette, Study of morphologies of PMMA/PP/PS ternary blends, Macromolecules 39 (2006) 2663–2675, https://doi.org/10.1021/ma052571n.

[45] S.H. Anastasiadis, I. Gancarz, J.T. Koberstein, Compatibilizing effect of block copolymers added to the polymer/polymer interface, Macromolecules 22 (1989) 1449–1453, https://doi.org/10.1021/ma00193a074.

[46] Y. Cao, P. Xu, B. Wu, M. Hoch, P.J. Lemstra, W. Yang, W. Dong, M. Du, T. Liu, P. Ma, High-performance and functional PBT/EVMG/CNTs nanocomposites from recycled sources by in situ multistep reaction-induced interfacial control, Compos. Sci. Technol. 190 (2020) 108043, https://doi.org/10.1016/j.compscitech.2020.108043.

[47] H. Wang, B. Wei, X. Gu, T. Lin, Y. Li, Determining the optimal molecular architecture for reactive splicing compatibilization: toward a better understanding of reactive polymer processing, Polymer 208 (2020) 122948, https://doi.org/10.1016/j.polymer.2020.122948.

[48] W. Dong, M. He, H. Wang, F. Ren, J. Zhang, X. Zhao, Y. Li, PLLA/ABS blends compatibilized by reactive comb polymers: double Tg depression and significantly improved toughness, ACS Sustain. Chem. Eng. 3 (2015) 2542–2550, https://doi.org/10.1021/acssuschemeng.5b00740.

[49] W. Lin, J.P. Qu, Enhancing impact toughness of renewable poly(lactic acid)/thermoplastic polyurethane blends via constructing cocontinuous-like phase morphology assisted by ethylene-methyl acrylate-glycidyl methacrylate copolymer, Ind. Eng. Chem. Res. 58 (2019) 10894–10907, https://doi.org/10.1021/acs.iecr.9b01644.

[50] S. Kashani Rahimi, R. Aeinehvand, K. Kim, J.U. Otaigbe, Structure and biocompatibility of bioabsorbable nanocomposites of aliphatic-aromatic copolyester and cellulose nanocrystals, Biomacromolecules 18 (2017) 2179–2194, https://doi.org/10.1021/acs.biomac.7b00578.

[51] K. Zhang, V. Nagarajan, M. Misra, A.K. Mohanty, Supertoughened renewable PLA reactive multiphase blends system: phase morphology and performance, ACS Appl. Mater. Interfaces 6 (2014) 12436–12448, https://doi.org/10.1021/am502337u.

[52] C.D. Han, D.M. Baek, J.K. Kim, T. Ogawa, N. Sakamoto, T. Hashimoto, Effect of volume fraction on the order-disorder transition in low molecular weight polystyrene-block-polyisoprene copolymers. 1. Order-disorder transition temperature determined by rheological measurements, Macromolecules 28 (1995) 5043–5062, https://doi.org/10.1021/ma00118a038.

[53] Y. Zhang, M. Zuo, Y. Song, X. Yan, Q. Zheng, Dynamic rheology and dielectric relaxation of poly(vinylidene fluoride)/poly(methyl methacrylate) blends, Compos. Sci. Technol. 106 (2015) 39–46, https://doi.org/10.1016/j.compscitech.2014.10.024.

[54] X.R. Gao, Y. Li, H.D. Huang, J.Z. Xu, L. Xu, X. Ji, G.J. Zhong, Z.M. Li, Extensional stress-induced orientation and crystallization can regulate the balance of toughness and stiffness of polylactide films: interplay of oriented amorphous chains and crystallites, Macromolecules 52 (2019) 5278–5288, https://doi.org/10.1021/acs.macromol.9b00932.

[55] Z.X. Huang, M.M. Wang, Y.H. Feng, J.P. Qu, Supertough, ultrastrong, and transparent poly(lactic acid) via directly hot pressing under cyclic compressing-releasing, Macromolecules 54 (2021) 4847–4853, https://doi.org/10.1021/acs.macromol.1c00530.

[56] Z. Liu, Y. Luo, H. Bai, Q. Zhang, Q. Fu, Remarkably enhanced impact toughness and heat resistance of poly(l -Lactide)/Thermoplastic polyurethane blends by constructing stereocomplex crystallites in the matrix, ACS Sustain. Chem. Eng. 4 (2016) 111–120, https://doi.org/10.1021/acssuschemeng.5b00816.